Check for updates

ChemSusChem

Research Article
doi.org/10.1002/cssc.202301242

Chemistry Europe
European Chemical Societies Publishing

www.chemsuschem.org

Special Collection

Ionic Liquid Boosting the Electrochemical Stability of a Poly(1,3-dioxolane) Gel Electrolyte for High-voltage Solid-State Lithium Batteries

Tianhua Chen,[a, b] Jiaxin Liu,[b, c] Dusan Losic,*[a] Jian Wang,*[d] and Haitao Zhang*[b]

Poor interfacial contact between solid-state electrolytes and electrodes limits high-voltage performance of solid-state lithium batteries. A new gel electrolyte is proposed via in-situ polymerization, incorporating fluoroethylene carbonate (FEC) solvent and ionic liquid1-butyl-1-methylpiperidinium bis(trifluoromethylsulfonyl)imide ($PP_{14}TFSI$). This combination synergistically enhances Li ion transport, achieving a transfer number of 0.58 and improved electrochemical performance. FEC protects the Al current collectors from $LiPF_6$ corrosion and promotes a protective interfacial layer formation. $PP_{14}TFSI$ improves interfacial contact and provides stable components. An interface layer of fluorine and nitrogen composites forms, preventing side reactions. $LiCoO_2$||PPE||Li cell exhibits robust cycling stability at 4.45 V, retaining ~80% capacity after 200 cycles at room temperature with 0.2 C and 1 C rates, showing increased coulombic efficiency. NCM811||PPE||Li cell also displays exceptional cycling. In-situ polymerization and FEC-ionic liquid coordination enable high-voltage solid-state lithium metal batteries for practical use.

1. Introduction

Solid-state lithium metal batteries (LMBs) have been a subject of interest for several years due to their high energy density and safety. They are considered as the next-generation rechargeable batteries.[1] By using solid-state electrolytes (SSEs), these batteries can overcome the safety hazards associated with low thermal stability, leakage, and flammability of organic liquid electrolytes, which is significant problem in commercial lithium-ion batteries.[2] However, the performance of high-voltage lithium metal batteries is hindered by interfacial issues,[3] low conductivity at room temperature, and narrow electrochemical windows of the electrolyte.[4]

Interfacial contact is an important factor in evaluating battery performance. One of the main challenges with lithium metal batteries is the formation of dendrites, which are microscopic, needle-like or mossy-like structures that can grow from the surface of the lithium metal electrode and penetrate the separator, causing short circuits and potentially leading to safety issues.[5] There are several factors that contribute to the formation of dendrites, including the uneven deposition of lithium metal on the electrode surface during charging, the formation of a solid electrolyte interphase (SEI) layer on the electrode surface, and the presence of impurities in the electrolyte. To address these issues, researchers are exploring a variety of strategies, including the use of electrolytes with additives that can improve the stability of the SEI layer, the development of new electrode materials that can reduce the formation of dendrites, and the use of advanced characterization techniques to better understand the fundamental processes that occur at the lithium metal-electrolyte interface.[6]

The use of in-situ polymeric electrolytes can result in higher conductivity and a reduction in interfacial impedance. Additionally, the liquid-state monomer (such as 1,3-dioxolane (DOL)[7] and vinyl carbonate[8]) used before polymerization has better wetting properties for the electrodes, improving the contact performance of interfaces and providing efficient pathways for the transmission of lithium ions.[9] To form high-purity solid-state electrolytes in assembled batteries, the liquid electrolytes are polymerized. However, the interface between the monomers and high-voltage cathode/high-capacity anode can cause unexpected side reactions, hindering the matching process.[9] To address this, researchers have proposed incorporating ionic

[a] Dr. T. Chen, Prof. D. Losic
School of Chemical Engineering and Advanced Materials
The University of Adelaide
Adelaide, SA-5005 (Australia)
E-mail: dusan.losic@adelaide.edu.au

[b] Dr. T. Chen, J. Liu, Prof. H. Zhang
Institute of Process Engineering
Chinese Academy of Sciences
100190, Beijing (P. R. China)
E-mail: htzhang@ipe.ac.cn

[c] J. Liu
College of Chemical Engineering
Shenyang University of Chemical Technology
Shenyang, 110142 (P. R. China)

[d] Dr. J. Wang
Helmholtz Institute Ulm (HIU)
89081 Ulm (Germany)
E-mail: jian.wang@kit.edu

Supporting information for this article is available on the WWW under https://doi.org/10.1002/cssc.202301242

Special Collection This publication is part of a joint Special Collection on Solid State Batteries, featuring contributions published in Advanced Energy Materials, Energy Technology, Batteries & Supercaps, ChemSusChem, and Advanced Energy and Sustainability Research.

© 2023 The Authors. ChemSusChem published by Wiley-VCH GmbH. This is an open access article under the terms of the Creative Commons Attribution License, which permits use, distribution and reproduction in any medium, provided the original work is properly cited.

© 2023 The Authors. ChemSusChem published by Wiley-VCH GmbH

liquids as high-conductive materials and liquid plasticizers into polymer matrices, which can increase the volume of amorphous regions and improve the electrochemical performance of LMBs.[10] Therefore, it provides pathways for the movement of Li^+ ions between polymer chains at room temperature. $PP_{14}TFSI$, an ionic liquid with a high electrochemical window (5.2 V) and high conductivity, has been utilized in rechargeable magnesium batteries, graphite dual-ion batteries, and Li/S batteries.[11] Fluoroethylene carbonate (FEC) can be used as an additive in the electrolyte of lithium-ion batteries. The role of FEC in lithium-ion batteries is to improve the contact between the electrolyte and electrodes, enhancing battery performance and stability. It can form a protective layer to reduce the volatilization and oxidation of the electrolyte, thereby reducing capacity loss and extending the battery life. In addition, FEC can also reduce the formation of SEI film on the electrode surface, improving battery cycling performance and fast charging capability.[12]

In this work, in-situ polymerized poly(1,3-dioxolane) fabricated with ionic liquid $PP_{14}TFSI$ and FEC (shorted for PPE electrolyte) has been proposed to improve key performances of Li metal batteries including high conductivity and Li transfer number of 0.58. To improve the energy density, an effective approach is to match high-potential difference and high-capacity cathodes, such as $LiCoO_2$ (LCO), with polymer electrolytes in Li metal batteries (LMBs). To our knowledge, solid-state lithium metal batteries capable of operating at 4.45 V are rarely seen with PDOL electrolyte system. The participation of FEC and ionic liquid enable stable interfacial layers between PPE electrolyte and electrodes.

Experimental Section

Materials

1-butyl-1-methylpiperidinium bis(trifluoromethylsulfonyl)imide ($PP_{14}TFSI$, 99.99%, Lanzhou Institute of Chemical Physics Co., Ltd.). 1,3-dioxolane (DOL, 99.99%, Sigma-Aldrich), 1,2-Dimethoxyethane (DME, 99.99%, Sigma-Aldrich), lithium bis(trifluoromethanesulfonyl)imide (LiTFSI, 99.99%, Sigma-Aldrich), Lithium hexafluorophosphate ($LiPF_6$, 99.99%, Sigma-Aldrich). $LiCoO_2$ (LCO, 4.45 V), $LiNi_{0.8}Co_{0.1}Mn_{0.1}O_2$ (NCM811) and $LiFePO_4$ (LFP) materials were bought from Guangdong Canrd New Energy Technology Co. Ltd.

Preparation of electrolyte, cathode, and assembly of battery

The polymeric electrolyte (PPE) was synthesized by mixing and in-situ polymerization of DOL monomer, 1 M LiTFSI salt, FEC solvent, DMC solvent, $PP_{14}TFSI$, PE separator, and 1 M $LiPF_6$ initiator at room temperature. The electrolyte without the addition of ionic liquids and FEC is named PDOL. The electrolyte with the addition of ionic liquids is named PPE electrolyte, and the content of FEC will be indicated as a percentage in front of it. The LCO or the LFP electrode was prepared by spreading a slurry of active material, super P, and polyvinylidene fluoride (PVDF) onto an Al current collector using a blade. The weight ratio of active material, super P, and PVDF was 8:1:1. The electrodes were then vacuum dried at 100 °C for 12 hours, cut into 14 mm diameter disks, and dried again at 100 °C in vacuum for 12 hours. The loading density of active materials on the cathode was 3~4 mg cm^{-2}. All the electrolyte preparation and battery assembly procedures were carried out at room temperature in an Ar-filled glove box. The cathode, pre-polymerized electrolyte, and Li metal anode were assembled in a CR 2025 coin cell.

Characterization

The Nicolet Avatar 360 Spectrometer was used to capture Fourier transform infrared spectroscopy (FT-IR) spectra within a range of 4000–500 cm^{-1}. The Hitachi SU8020 scanning electron microscope (SEM) and Transmission electron microscopy (TEM, JEM-2100HR, Japan) was used to examine the surface morphology structure of the samples. In order to examine alterations in both the surface and underlying composition of recycled lithium metal and cathode, X-ray photoelectron spectroscopy (XPS) was conducted using the Thermo Fisher Scientific ESCALAB 250 Xi apparatus with Al Ka radiation (hv = 1486.6 eV) as the X-ray source. ^{7}Li NMR measurements were conducted on a JNM-ECZ600R with a resonance frequency of 233 MHz. The differential scanning calorimetry (DSC) was performed with a heating rate of 5 °C min^{-1} to measure their thermal properties by thermogravimetric (Setaram Labsys).

Electrochemical measurements

The constant-currents charge and discharge cycling performances of Li||PPE||LCO/LFP/NCM811 half cells were tested with a LAND test system (CT2001 A, China) with a working voltage of 2.5–4.45 V, 2.5–4.0 V, 2.8–4.3 V, separately. The Li||PPE||LCO rate test of charge-discharge current was set at the ones corresponding to C/5, 1 C, (1 C = 178 mA g^{-1}) without using a constant-voltage mode at both ends of charge and discharge. The Li||PEE||Li symmetric cells were packed with 16 mm Li metal foil, and the tests were operated by Land setting for galvanostatic cycling with current densities of 0.2, 0.5, 1 mA cm^{-2}, respectively. An Li||PPE||stainless steel (ss) asymmetrical cell was employed for linear scanning voltammetry (LSV), with the working electrode consisting of a stainless-steel sheet as the working electrode, Li foil as the counter electrode and reference electrode, in the Autolab (PGSTAT302 N) electrochemical workstation at a scanning rate of 1 mV s^{-1}. The LSV were collected in 2.0–6.0 V. Electrochemical impedance spectroscopy (EIS) was carried out in the CHI660E under an open circuit voltage, with a frequency range of 10^5–10^{-2} Hz and an amplitude of 5 mV. All the above tests were carried out at 25 °C. The electrochemical floating analysis experiment was conducted by performing constant current and constant voltage tests on the NCM622||PMI||Li battery. The battery was charged with a constant current of 0.05 mA to 4.0 V initially, then charged with 4.0 V for 10 hours, and continuously charged with a constant current 0.05 mA to 4.1 V and held for 10 hours. This process was repeated until the voltage reached to 5.0 V. All the Li battery cycles and battery cycling performance were conducted on a Neware or LAND battery cycler. The transference number (t_{Li^+}) of the battery was determined via chronoamperometry using a constant polarization potential of 10 mV at 60 °C. The calculating equation of t_{Li^+} is: $t_{Li^+} = [I_S(\Delta V - R_0 I_0)]/[I_0(\Delta V - R_S I_S)]$, where I_o and I_s correspond to the initial and steady-state currents, R_o and R_s represent the interface resistances before and after polarization. All the Li battery cycles and battery cycling performance were conducted on a Xinwei or LAND battery cycler.

© 2023 The Authors. ChemSusChem published by Wiley-VCH GmbH

1864564x, 2024, 5, Downloaded from https://chemistry-europe.onlinelibrary.wiley.com/doi/10.1002/cssc.202301242 by Karlsruher Institut F., Wiley Online Library on [22/11/2024]. See the Terms and Conditions (https://onlinelibrary.wiley.com/terms-and-conditions) on Wiley Online Library for rules of use; OA articles are governed by the applicable Creative Commons License

2. Results and Discussion

2.1. In-situ polymerization

The liquid-state electrolyte can be infused into porous electrodes via in-situ polymerization, leading to their conversion into solid-state electrolytes (PPE) within porous channels of the electrode, as depicted in Figure 1. Therefore, the mass percentage of active materials in the electrodes produced by in-situ polymerization is similar to that of traditional liquid-state batterie. The images in Figure S1a-b display SEM views of the electrode before and after undergoing in-situ polymerization. The images reveal that the LCO electrode was uniformly coated with a layer of PPE, which was not present in the initial LCO electrode.

Fourier transform infrared spectroscopy (FT-IR) was employed to examine the changes in functional groups of the electrolyte after polymerization, as illustrated in Figure 2a. It seems that the distinct peaks of the cyclic ether in DOL, which were found at 925 and 1096 cm^{-1}, were noticeably absent after the polymerization process.[13] Instead, a sudden appearance of a characteristic peak around 845 cm^{-1} for the O–C–O chains in PDOL was observed, indicating a successful polymerization process with inevitable DOL monomer retention, as reported.[14] Furthermore, the shifting of the C–O–C vibration at 1010 and 1090 cm^{-1} and the lack of $–CH_2–$ vibration between 2800 to 3000 cm^{-1} signify that long chain is formed through DOL ring-opening polymerization.[15] The effects of FEC addition on the structure of PDOL segments were investigated in the study. The feature peaks of FEC between 1750~1800 cm^{-1} illustrates that that there was no chemical reaction between FEC and DOL when undergoing in situ polymerization.[16] The structure and composition information are also confirmed by the ^{1}H and ^{13}C NMR spectra in Figure 3b–c. It is notable that the hydrogen

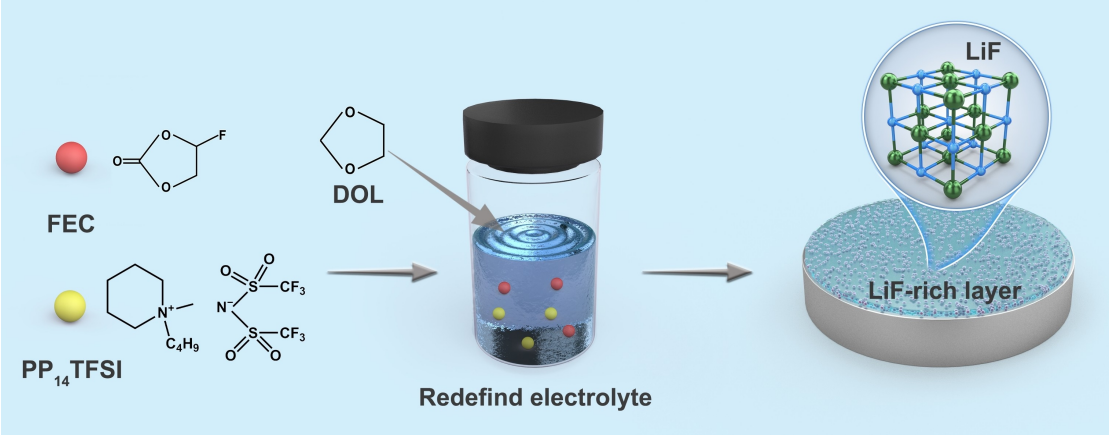

Figure 1. Schematic diagram of the in-situ polymerization process in the battery.

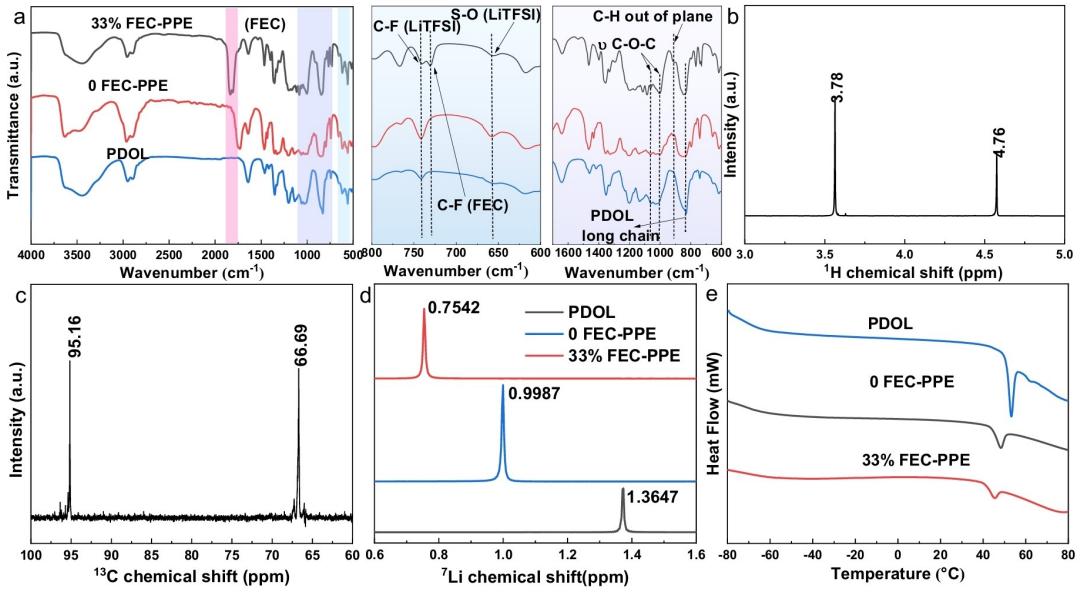

Figure 2. (a) FTIR spectra of in-situ polymerization (PDOL, PPE electrolyte) samples at room temperature, (b) ^{1}H NMR of in-situ polymerization of PPE, (c) ^{13}C NMR of in-situ polymerization of PPE, (d) ^{7}Li NMR of in-situ polymerization (PDOL, 0 FEC-PPE, and 33% FEC-PPE electrolyte) samples, all the sample were applied deuterated acetone as solvent, (e) DSC curves of PDOL and PPE samples.

© 2023 The Authors. ChemSusChem published by Wiley-VCH GmbH

1864564x, 2024, 5, Downloaded from https://chemistry-europe.onlinelibrary.wiley.com/doi/10.1002/cssc.202301242 by Karlsruher Institut F., Wiley Online Library on [22/11/2024]. See the Terms and Conditions (https://onlinelibrary.wiley.com/terms-and-conditions) on Wiley Online Library for rules of use; OA articles are governed by the applicable Creative Commons License

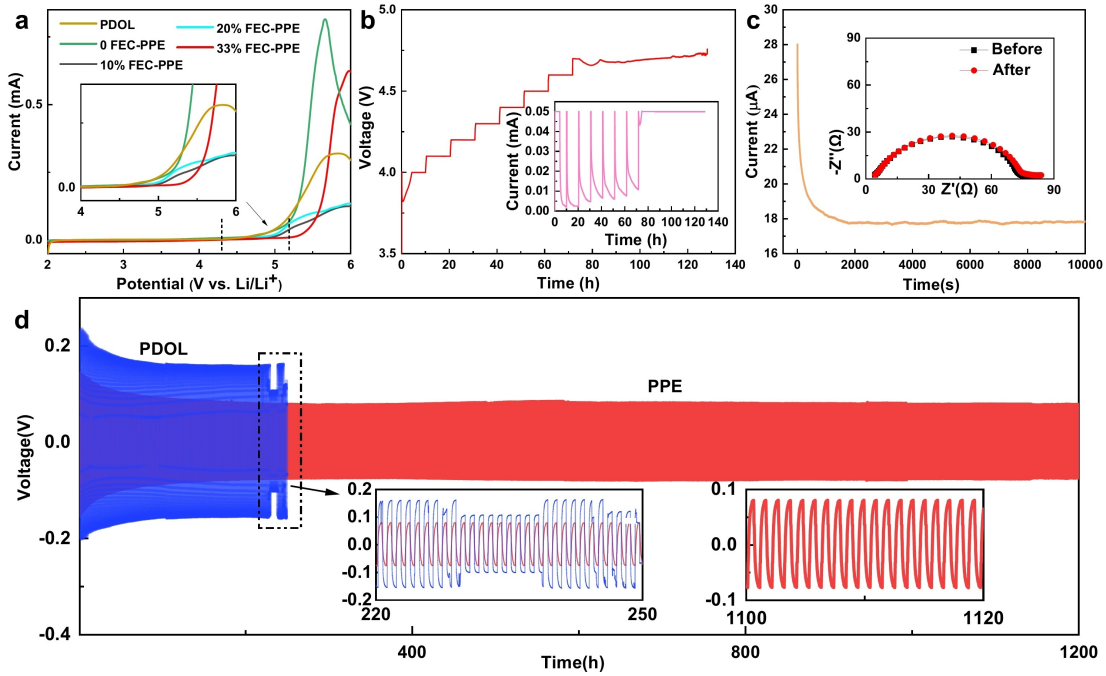

Figure 3. (a) LSV measurements of diffent electrolytes, (b) electrochemical floating analysis of NCM622||PPE||Li battery, (c) current-time curve following DC polarization curves of the PPE electrolyte at room temperature (inset: EIS variation at initial and steady states). (d) Voltage profiles of Li||PPE||Li symmetrical cellat 0.2 mA cm^{-2}, and 0.2 mA h cm^{-2} and room temperature.

peaks exhibit chemical shifts after polymerization, the peak at 3.78 and 4.76 ppm corresponds to the H on –O–CH_2–CH_2–O– and –O–CH_2–O– group, respectively.[17] The peak of ^{13}C NMR spectra at 66.69 and 95.16 ppm corresponds to C on group –O–CH_2–CH_2–O– and –O–CH_2–O– separately. These are consistent with the PDOL structure.[18] Furthermore, the results of FTIR and NMR analyses suggest that there was no chemical reaction between FEC, IL, and DOL during the in situ polymerization of DOL. The incorporation of FEC and IL into the PDOL chain framework resulted in the formation of the amorphous region, which led to a reduction in the degree of polymer crystallization. This effect is clearly noticeable in the DSC findings, shown in Figure 2e. The ^{7}Li NMR compares the chemical shift of PDOL, 0 FEC-PPE, and 33 % FEC-PPE electrolyte sample. The left shift of the peaks represents the increased mobility of Li^+, improved the performance of the battery.

2.2. Electrochemical tests of PPE electrolyte

Linear sweep voltammetry (LSV) was applied to examine the electrochemical window of the electrolyte that were polymerized in situ, the results are shown in Figure 3a. It can be observed that the PPE has an electrochemical window wider than 5.2 V. It is obviously that he addition of FEC and PP_{14}TFSI. Due to the effects of FEC and IL in increasing the operating voltage window of the electrolyte, the electrochemical window of the PPE electrolyte has been significantly enhanced. This is also partly due to the ring-opening polymerization of DOL, which results in the formation of long linear chains.[15] The wider electrochemical window of the PPE suggests that it can be effectively paired with high-voltage cathodes such as LCO and NCM811. The result of the electrochemical floating experiment using NCM622||PPE||Li battery shows that the battery can still operate stably when the voltage reaches 4.6 V (Figure 3b). When the charge voltage is higher than 4.6 V, which exceeds the voltage window that the electrolyte can withstand, will accelerate the electrolyte decomposition process. Overvoltage charging for the Li anode of the battery means trying to squeeze an excessive number of Li ions into its limited space, resulting in the inability of the Li ions to embed and depositing on the electrode surface, leading to the formation of dendritic growth. As for the cathode, too many Li ions are driven to depart from the cathode lattice structure, affecting the stability of its structure and causing local collapse.

The t_{Li^+} value was calculated and the chronoamperometry curves is shown in Figure 3c, which is 0.58 for the PPE electrolyte, much higher than the PDOL. Effectively increased t_{Li^+} can result in a reduction of concentration polarization for Li^+, prevent the formation of lithium dendrites, and enable faster charging/discharging rates. The enhancement of t_{Li^+} can be attributed to the abundance of free Li ions created by the synergistic effect between the FEC and PP_{14}^+ groups in IL, as confirmed by FTIR, NMR and the following XPS results.

To assess the reversibility of Li plating/stripping in different electrolytes, Li||Li symmetric batteries were tested at room temperature at different current density, as shown in Figure 3d and Figure S2–S3. At a current density of 0.2 mA cm^{-2}, the PDOL exhibited a larger initial overpotential about 0.45 V, and undergo a short circuit after 230 h. This implies the unstable interfacial contact, which is caused by the higher polymer-

© 2023 The Authors. ChemSusChem published by Wiley-VCH GmbH

1864564x, 2024, 5, Downloaded from https://chemistry-europe.onlinelibrary.wiley.com/doi/10.1002/cssc.202301242 by Karlsruher Institut F., Wiley Online Library on [22/11/2024]. See the Terms and Conditions (https://onlinelibrary.wiley.com/terms-and-conditions) on Wiley Online Library for rules of use; OA articles are governed by the applicable Creative Commons License

ization degree of the PDOL. While for the battery with PPE electrolyte, the initial overpotential was about 0.3 V, which slowly reduced to 0.15 V after 100 h, and remained stable for 1200 h. The large initial overpotential may be caused by the small amount of unpolymerized DOL monomers, which reversed to promote a close interfacial contact, resulting in a stable cycling performance. When the current density increased to 0.5 and 1 mA cm^{-2}, the overpotential increased significantly to 0.2 and 0.3 V, separately (Figure S2 and Figure S3). The Li||PPE||Li cell demonstrated stable performance at 1 mA cm^{-2}, with no significant increase in polarization even after 100 hours of cycling (as illustrated in Figure S3). This suggests that the system has good compatibility and stability with the Li anode, which is capable of effectively preventing the growth of dendritic lithium.

2.3. Characterization of electrolyte-anode interface

The post-symmetric cells, which contained different electrolytes, undergo 50 cycles at a rate of 0.2 mA cm^{-2} for 0.2 mA h cm^{-2}. Afterwards, the cells were taken apart to observe the surface morphology of the extracted Li metals through SEM, as shown in Figure 4a-b. It is notable that there was mossy lithium dendrite on the PDOL Li anode, while the surface of PPE cycled Li anode was flat and smooth without lithium dendrite. This phenomenon is consistent with the Li symmetry cycling performance. The chemical composition of the solid electrolyte interphase (SEI) on Li anode obtained from cycled Li||PPE||Li cells was investigated via XPS. This analysis was carried out after subjecting the cells to 100 hours of cycling at a current density of 0.2 mA cm^{-2}, with PDOL and PPE electrolyte, separately (Figure 4c-h). The C 1s spectra (shown in Figure 4c) indicate that the SEI layer on Li metal from PDOL battery is responsible for the C–O peak (286.33 eV) and O=C–O peak (289.44 eV). These peaks correspond to the breakdown of DME solvent.[19] The peaks of F 1s at 685.2 and 686.7 eV are assigned to LiF and $Li_xPF_yO_z$, respectively, resulting from the decomposition of $LiPF_6$ salt (Figure 4e). It has been reported that the SEI layer from a typical $LiPF_6$ system is unstable to support long stability and the $LiPF_6$ corrodes the current collector.[20] FEC has been suggested as a viable electrolyte supplement that boosts the firmness and

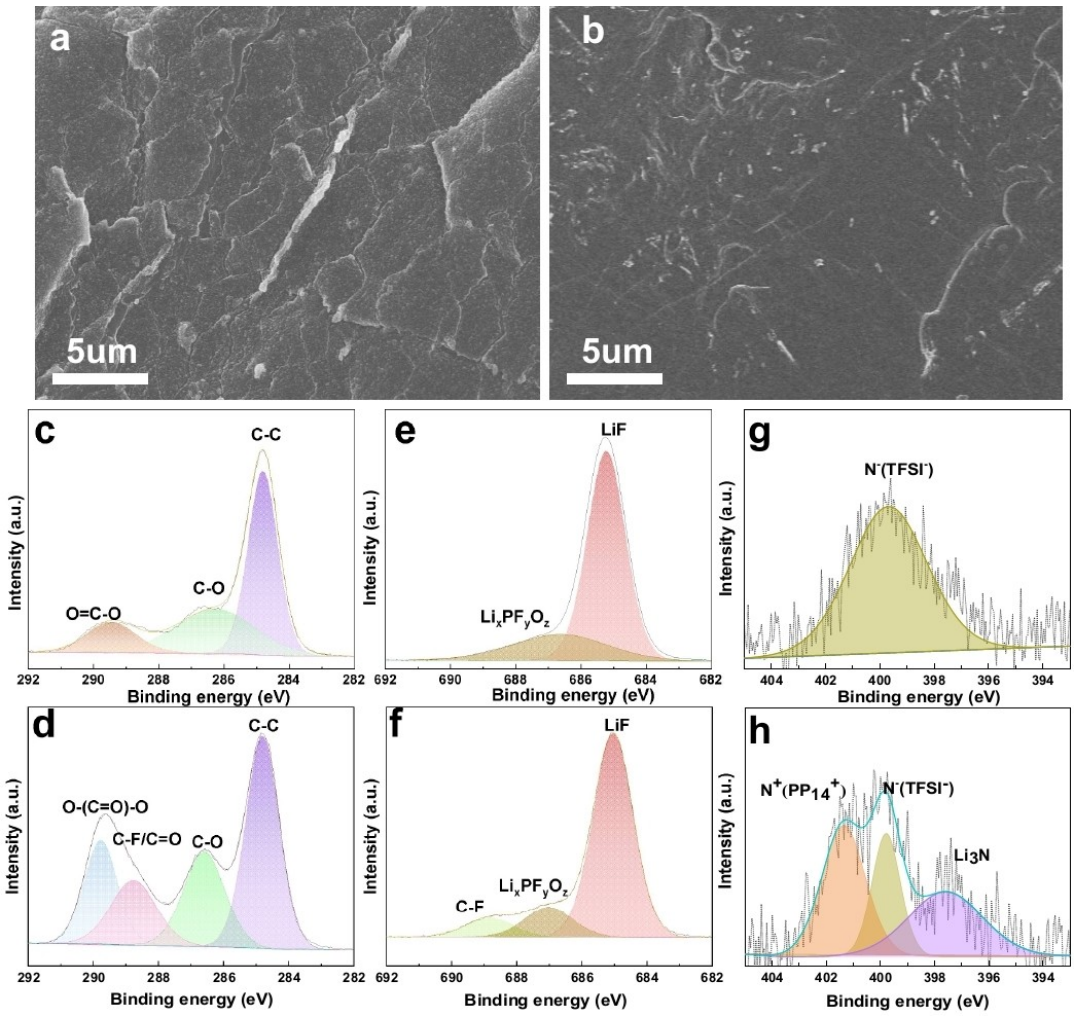

Figure 4. SEM images of Li anode amphogy with (a) PDOL electrolyte, (b) PPE electrolyte, XPS spectra (C 1s, F 1s, N 1s) of the Li metal surface from the cycled Li||Li symmetric cells after 50 cycles at 0.2 mA cm^{-2} (c, e, g) PDOL electrolye, and (d, f, h) PPE electrolyte.

© 2023 The Authors. ChemSusChem published by Wiley-VCH GmbH

1864564x, 2024, 5, Downloaded from https://chemistry-europe.onlinelibrary.wiley.com/doi/10.1002/cssc.202301242 by Karlsruher Institut F., Wiley Online Library on [22/11/2024]. See the Terms and Conditions (https://onlinelibrary.wiley.com/terms-and-conditions) on Wiley Online Library for rules of use; OA articles are governed by the applicable Creative Commons License

1864564x, 2024, 5, Downloaded from https://chemistry-europe.onlinelibrary.wiley.com/doi/10.1002/cssc.202301242 by Karlsruher Institut F., Wiley Online Library on [22/11/2024]. See the Terms and Conditions (https://onlinelibrary.wiley.com/terms-and-conditions) on Wiley Online Library for rules of use; OA articles are governed by the applicable Creative Commons License

flexibility of the solid electrolyte interphase (SEI) in Li metal anodes.[21] It has a good ability to stabilize lithium metal negative electrode and can form a dense SEI with high LiF content on the metal lithium negative electrode. Furthermore, FEC additive can alleviate the corrosion of $LiPF_6$ on the battery and help to form stable SEI on the anode and CEI on the cathode.[22] As illustrated in Figure 4d and f, the existence of FEC leads to the formation of LiF (685.2 eV) and C–F (688.8 eV) coating the surface of Li metal. The LiF found in the solid electrolyte interphase (SEI) layer possesses a high level of mechanical strength and interface energy, which aids in improving the mechanical resilience of the SEI and prevents the growth of lithium dendrites. In addition, the decomposition of FEC on the Li metal causes the emergence of the C–O peak (286.6 eV), C–F/C=O peak (288.7 eV), and O–(C=O)–O peak (289.9 eV) within the SEI layer, as observed in the C 1s spectra.[12]

In N 1s spectra, the peak at approximately 399.8 eV is linked to imide groups found in LiTFSI salt or $PP_{14}TFSI$, as shown in Figure 4g and h. Meanwhile, the presence of N^- in Li_3N and N^+ in PP_{14}^+ results in two additional peaks at 397.5 and 401.3 eV, separately.[23] As a result, the $PP_{14}TFSI$ ionic liquid in the PPE electrolyte system modifies the SEI layers on the Li metal surface, creating a protective interphase that remains stable during cycling and reduces side reactions between the electrolyte and Li metal. Moreover, PPE electrolyte system promotes the production of Li_3N during cycling, which helps to prevent the growth of Li dendrites. In addition, it can be deduced that the $PP_{14}TFSI$ ionic liquid has the ability to wet the interface, increase the electrochemical window, and reduce the crystallinity of the polymer. The interface of the electrolytes and electrodes is an important factor in measuring battery performance.

There is no signal indicating the decomposition of DOL monomer, and PDOL which confirms that the SEI rich in LiF resulting from FEC decomposition can effectively prevent the reaction between the electrolyte and lithium metal, ultimately leading to improved electrochemical performance. The improved cycling performance of Li||PPE||Li cells, which have dendrite-free and compact lithium on the lithium metal surface, can be explained by the presence of a stable LiF riched SEI, excellent interfacial contact, and a reduced Li nucleation overpotential. These factors coordinated to protect the lithium anode and prevent the growth of dendritic lithium.

2.4. Cycling performance matched with high-voltage cathodes

With high Li^+ transport and remarkable stability towards lithium metal at room temperature, the PPE electrolyte enable high voltage performance of batteries with different cathodes. Batteries with a high-voltage and capacity $LiCoO_2$ cathode were assembled and tested from 3 to 4.45 V at room temperature. Figure 5 show the cycling performance of LCO ||PEE||Li batteries with PPE at room temperature (25 °C). After being activated for 5 cycles at 0.1 C, the initial discharge specific capacity of $LiCoO_2$||PPE||Li at 0.2 C is 167.5 mAh g^{-1}, higher than that of $LiCoO_2$||PDOL||Li battery (Figure S4), showing a better compatibility against high-voltage cathodes. And the capacity retain is 78.9% after 200 cycles (88.6% after 100th), with a stable Coulombic efficiency. As a contrast, the $LiCoO_2$||PDOL||Li battery decayed sharply and suffered unstable Coulombic efficiency. The discharge specific capacity of $LiCoO_2$||PPE||Li battery is 174.2, 167.5, 154.2, 140.5, and 107.8 mAh g^{-1}, corresponding to 0.1 C, 0.2 C, 0.5 C, 1 C, and 2 C, respectively. Figure S5 display the TEM image of $LiCoO_2$ cathode after cycled for 20 cycles at 0.1 C, the CEI layer is uniform and with a thickness of 12 nm. The CEI, which is both thin and robust, has the dual capability of inhibiting undesirable reactions between the cathode and electrolyte, as well as lowering the energy barrier for the diffusion of Li ions on the surface.

NCM811 cathode was also applied to test value the PPE electrolyte at room temperature, as depicted in Figure 6. NCM811||PPE||Li batteries were assembled and tested from 3 to 4.3 V at room temperature. The discharge specific capacity of NCM811||PPE||Li cell is 181.9, 162.7, 144.7, 143.6, 117.4 mA h g^{-1}, corresponding to 0.1 C, 0.5 C, 1 C, 2 C, 5 C, respectively (Figure 6b). With a high and stable Coulombic efficiency, the NCM811||PPE||Li cell exhibits excellent cycling performance at 1 C, from the initial 139.5 mA h g^{-1} to 130.2 mA h g^{-1} after 140 cycles, as shown in Figure 6c. The capacity retain is 93.3% with slight decay in each cycle, and the average Coulombic efficiency is 99.9%, indicating high compatibility of PPE electrolyte and NCM811 cathode. The TEM image of NCM811 after cycled at 0.1 C for 10 cycles demonstrates an even and uniform CEI layer with a thickness of only 8 nm.

The PPE has played a crucial role In enhancing the cycling performance of the $LiCoO_2$||Li or NCM811||Li cell by effectively preventing undesirable reactions between the in-situ polymerization electrolyte and electrodes. It was made possible by the presence of the protective interfacial layer consisting of nitrogen and fluorine composites offered by FEC solvent and $PP_{14}TFSI$. The synergistic effect of FEC and ionic liquid $PP_{14}TFSI$ results in the formation of a stable interfacial layer in the battery, thereby leading to excellent electrochemical performance.

3. Conclusions

In summary, a new gel electrolyte by in-situ polymerization, which involves the addition of the FEC solvent and ionic liquid PP14TFSI, is developed and demonstrated. The inclusion of FEC solvent and $PP_{14}TFSI$ was demonstrated for a multiple purpose in this system, leading to rapid propagation of lithium ions and good electrochemical performance. FEC has the role of impeding current collector corrosion resulting from $LiPF_6$, as well as encouraging the formation of a passivate interfacial layer at room temperature. On other hand, the $PP_{14}TFSI$ has a positive effect on enhancing interfacial contact, and offering stable components for the interfacial layer. During the electrochemical process, an interfacial layer is formed that contains fluorine and nitrogen composites, effectively inhibiting side

© 2023 The Authors. ChemSusChem published by Wiley-VCH GmbH

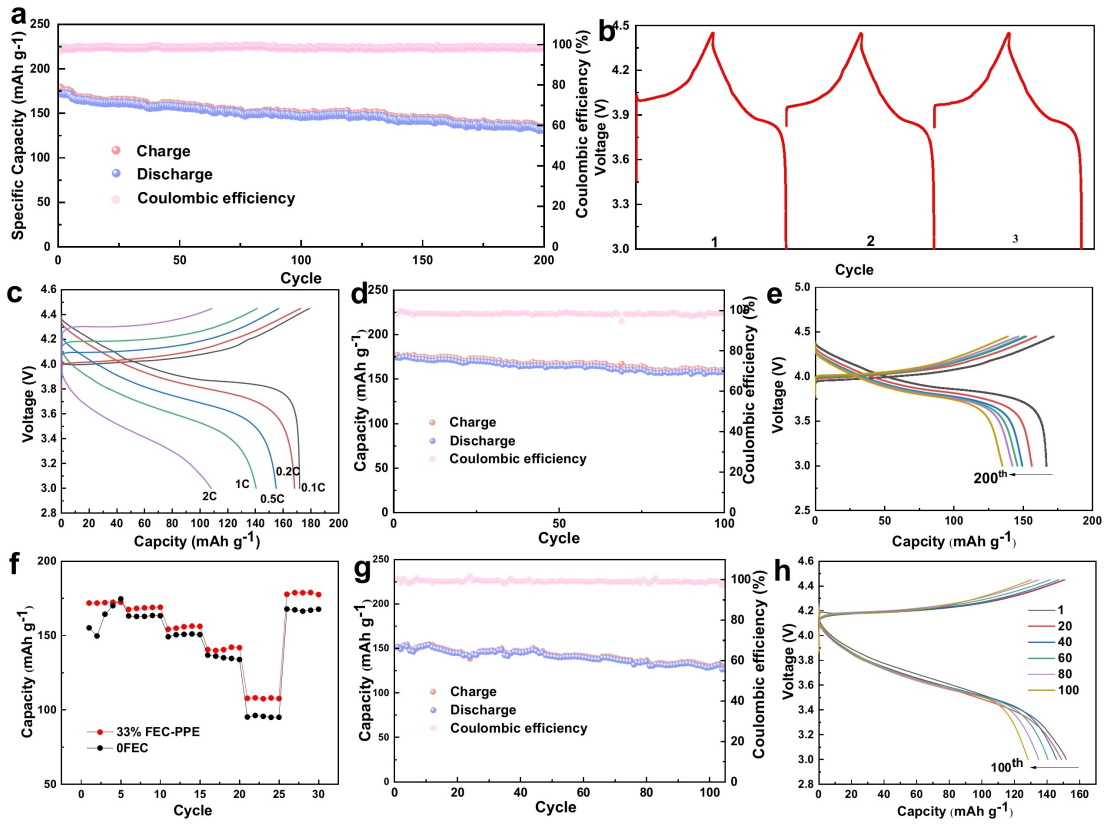

Figure 5. Electrochemical performance of $LiCoO_2$||PPE||Li cells: (a) Cycling performance at 0.2 C, (b) voltage file, (c) galvanostatic charge/discharge curve at different rates, (d) cycling performance of at 0.1 C, (e) galvanostatic charge/discharge curve at 0.2 C, (f) rate performance of, (g) at 1 C, (h) galvanostatic charge/discharge curve at 1 C. All the tests were conducted at room temperature.

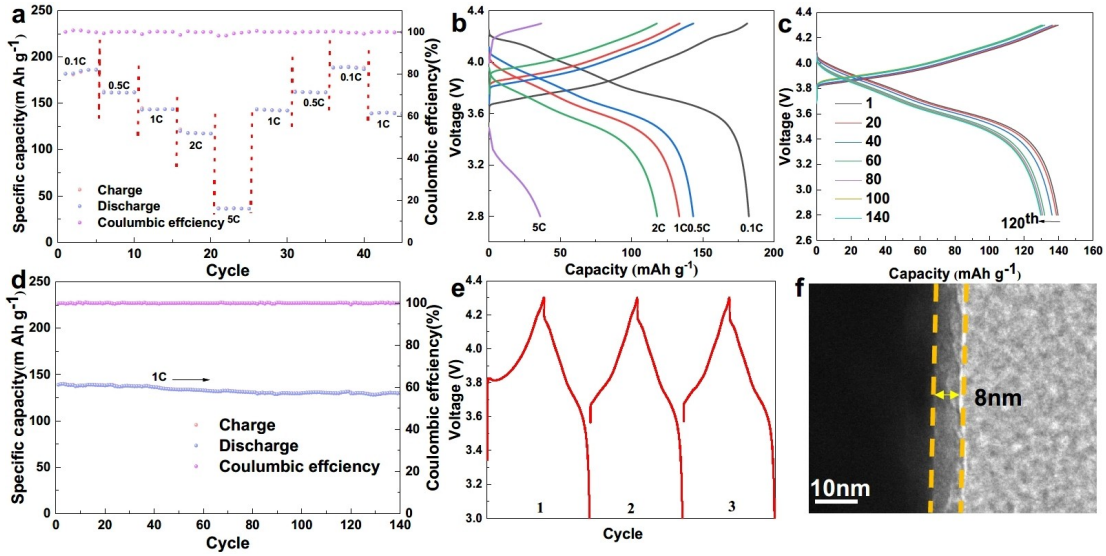

Figure 6. Electrochemical performance of NCM811||PPE||Li cells: (a) Rate performance, (b) galvanostatic charge/discharge curve at different rates, (c) galvanostatic charge/discharge curve at 1 C, (d) cycling performance of at 1 C, (e) voltage file, (f) TEM image of NCM811 after cycled at 0.1 C for 10 cycles. All the tests were conducted at room temperature.

reactions at the interface between the in-situ polymerization electrolyte and electrodes. The $LiCoO_2$||PPE||Li cell exhibits good cycling performance at a high voltage of 4.45 V, with a capacity retention of around 80% after 200 cycles at 0.2 C and 1 C room temperature, and a significant improvement in coulombic efficiency. The NCM811||PPE||Li cell also conducts excellent cycling performance. Overall, the use of in-situ polymerization and proposed effect of FEC and ionic liquid

© 2023 The Authors. ChemSusChem published by Wiley-VCH GmbH

1864564x, 2024, 5, Downloaded from https://chemistry-europe.onlinelibrary.wiley.com/doi/10.1002/cssc.202301242 by Karlsruher Institut F., Wiley Online Library on [22/11/2024]. See the Terms and Conditions (https://onlinelibrary.wiley.com/terms-and-conditions) on Wiley Online Library for rules of use; OA articles are governed by the applicable Creative Commons License

have the potential to enable the design of solid-state lithium metal batteries with high voltage for practical application.

Acknowledgements

The authors thank the Australian Government for providing Tianhua Chen with Beacon of Enlightenment PhD Scholarship to undertake PhD at the University of Adelaide and Institute of Process Engineering, Chinese Academy of Sciences. Dr. Jian Wang thanks the fellowship supported by Alexander von Humboldt Foundation. This work was partly supported by Australian Research Council (ARC), ARC research Hub for Graphene enabled industry transformation (IH 150100003), ZhongKe-YuNeng Joint R&D center (No. ZKYN2022006), the International Cooperative Project of CAS (No.122111-KYSB20210012), and the the Natural Science Foundation of Jiangsu Province (BK. 20210130), Innovative and Entrepreneurial Doctor in Jiangsu Province (JSSCBS20211428). Open Access funding enabled and organized by Projekt DEAL.

Conflict of Interests

The authors declare that they have no known competing financial interests or personal relationships that could have appeared to influence the work reported in this paper.

Data Availability Statement

The data that support the findings of this study are available on request from the corresponding author. The data are not publicly available due to privacy or ethical restrictions.

Keywords: Ionic liquid · In-situ polymerization · FEC solvent · High-voltage · Interfacial layer

[1] J. Liang, J. Luo, Q. Sun, X. Yang, R. Li, X. Sun, *Energy Storage Mater.* **2019**, *21*, 308–334.
[2] a) Y. Zheng, Y. Yao, J. Ou, M. Li, D. Luo, H. Dou, Z. Li, K. Amine, A. Yu, Z. Chen, *Chem. Soc. Rev.* **2020**, *49*, 8790–8839; b) S. Ma, M. Jiang, P. Tao, C. Song, J. Wu, J. Wang, T. Deng, W. Shang, *Prog. Nat. Sci. Mater. Int.* **2018**, *28*, 653–666.
[3] Q. Yang, J. Huang, Y. Li, Y. Wang, J. Qiu, J. Zhang, H. Yu, X. Yu, H. Li, L. Chen, *J. Power Sources* **2018**, *388*, 65–70.
[4] a) S. Xu, Z. Sun, C. Sun, F. Li, K. Chen, Z. Zhang, G. Hou, H.-M. Cheng, F. Li, *Adv. Funct. Mater.* **2020**, *30*, 2007172; b) Y. Wang, Y. Wu, Z. Wang, L. Chen, H. Li, F. Wu, *J. Mater. Chem. A* **2022**, *10*, 4517–4532.
[5] Y.-Y. Sun, F. Li, P.-Y. Hou, *J. Mater. Chem. A* **2021**, *9*, 9481–9505.
[6] K. Xu, *Chem. Rev.* **2014**, *114*, 11503–11618.
[7] a) J.-Y. Liang, X.-D. Zhang, X.-X. Zeng, M. Yan, Y.-X. Yin, S. Xin, W.-P. Wang, X.-W. Wu, J.-L. Shi, L.-J. Wan, Y.-G. Guo, *Angew. Chem. Int. Ed.* **2020**, *59*, 6585–6589; b) Q. Ma, J. Yue, M. Fan, S.-J. Tan, J. Zhang, W.-P. Wang, Y. Liu, Y.-F. Tian, Q. Xu, Y.-X. Yin, Y. You, A. Luo, S. Xin, X.-W. Wu, Y.-G. Guo, *Angew. Chem. Int. Ed.* **2021**, *60*, 16554–16560; c) Q. Liu, B. Cai, S. Li, Q. Yu, F. Lv, F. Kang, Q. Wang, B. Li, *J. Mater. Chem. A* **2020**, *8*, 7197–7204; d) T. Yang, W. Zhang, Y. Liu, J. Zheng, Y. Xia, X. Tao, Y. Wang, X. Xia, H. Huang, Y. Gan, X. He, J. Zhang, *Small* **2023**, *19*, 2303210.
[8] Q. Zhou, C. Fu, R. Li, X. Zhang, B. Xie, Y. Gao, G. Yin, P. Zuo, *Chem. Eng. J.* **2022**, *437*, 135419.
[9] Q. Zhao, X. Liu, S. Stalin, K. Khan, L. A. Archer, *Nat. Energy* **2019**, *4*, 365–373.
[10] a) X. Tang, S. Lv, K. Jiang, G. Zhou, X. Liu, *J. Power Sources* **2022**, *542*, 231792; b) G. Yang, Y. Song, Q. Wang, L. Zhang, L. Deng, *Mater. Des.* **2020**, *190*, 108563.
[11] a) W. Ren, D. Wu, Y. NuLi, X. Zhang, J. Yang, J. Wang, *ACS Appl. Mater. Interfaces* **2021**, *13*, 32957–32967; b) Z. Zhao-Karger, X. Zhao, D. Wang, T. Diemant, R. J. Behm, M. Fichtner, *Adv. Energy Mater.* **2015**, *5*, 1401155; c) J. Fan, Z. Zhang, Y. Liu, A. Wang, L. Li, W. Yuan, *Chem. Commun.* **2017**, *53*, 6891–6894.
[12] X.-Q. Zhang, X.-B. Cheng, X. Chen, C. Yan, Q. Zhang, *Adv. Funct. Mater.* **2017**, *27*, 1605989.
[13] H. Yang, B. Zhang, M. Jing, X. Shen, L. Wang, H. Xu, X. Yan, X. He, *Adv. Energy Mater.* **2022**, *12*, 2201762.
[14] J. Zhou, T. Qian, J. Liu, M. Wang, L. Zhang, C. Yan, *Nano Lett.* **2019**, *19*, 3066–3073.
[15] J. Yu, X. Lin, J. Liu, J. T. T. Yu, M. J. Robson, G. Zhou, H. M. Law, H. Wang, B. Z. Tang, F. Ciucci, *Adv. Energy Mater.* **2022**, *12*, 2102932.
[16] Z. Li, W. Tang, Y. Deng, M. Zhou, X. Wang, R. Liu, C.-a. Wang, *J. Mater. Chem. A* **2022**, *10*, 23047–23057.
[17] J. Ma, Y. Wu, H. Jiang, X. Yao, F. Zhang, X. Hou, X. Feng, H. Xiang, *Energy Environ. Mater.* **2022**, *6*, e12370.
[18] K. Khan, Z. Tu, Q. Zhao, C. Zhao, L. A. Archer, *Chem. Mater.* **2019**, *31*, 8466–8472.
[19] Z. Geng, Y. Huang, G. Sun, R. Chen, W. Cao, J. Zheng, H. Li, *Nano Energy* **2022**, *91*, 106679.
[20] C.-C. Su, M. He, R. Amine, Z. Chen, R. Sahore, N. Dietz Rago, K. Amine, *Energy Storage Mater.* **2019**, *17*, 284–292.
[21] T. Hou, G. Yang, N. N. Rajput, J. Self, S.-W. Park, J. Nanda, K. A. Persson, *Nano Energy* **2019**, *64*, 103881.
[22] Q. Wu, M. T. McDowell, Y. Qi, *J. Am. Chem. Soc.* **2023**, *145*, 2473–2484.
[23] J. Zheng, M. Gu, H. Chen, P. Meduri, M. H. Engelhard, J.-G. Zhang, J. Liu, J. Xiao, *J. Mater. Chem. A* **2013**, *1*, 8464–8470.

Manuscript received: August 22, 2023
Revised manuscript received: September 28, 2023
Accepted manuscript online: October 28, 2023
Version of record online: November 20, 2023

© 2023 The Authors. ChemSusChem published by Wiley-VCH GmbH

1864564x, 2024, 5, Downloaded from https://chemistry-europe.onlinelibrary.wiley.com/doi/10.1002/cssc.202301242 by Karlsruher Institut F., Wiley Online Library on [22/11/2024]. See the Terms and Conditions (https://onlinelibrary.wiley.com/terms-and-conditions) on Wiley Online Library for rules of use; OA articles are governed by the applicable Creative Commons License